J|A|C|S
ARTICLES

# First Hyperpolarizability Dispersion of the Octupolar Molecule Crystal Violet: Multiple Resonances and Vibrational and Solvation Effects

Jochen Campo,[†] Anna Painelli,[‡] Francesca Terenziani,[‡] Tanguy Van Regemorter,[§] David Beljonne,[§] Etienne Goovaerts,[†] and Wim Wenseleers[†,*]

*Department of Physics, University of Antwerp (campus Drie Eiken), Universiteitsplein 1, B-2610 Antwerpen, Belgium, Dipartimento di Chimica GIAF and INSTM UdR-Parma, Università di Parma, Parco Area delle Scienze 17/a, 43100 Parma, Italy, and Chemistry of Novel Materials, Center for Research in Molecular Electronics and Photonics, University of Mons, Place du Parc 20, B-7000 Mons, Belgium*

Received June 25, 2010; E-mail: Wim.Wenseleers@ua.ac.be

***Abstract:*** The first hyperpolarizability ($\beta$) dispersion curve is measured for the first time for an octupolar nonlinear optical (NLO) molecule (crystal violet, CV) and modeled theoretically, yielding an in-depth understanding of the electronic structure and vibronic and solvation effects on such octupolar conjugated systems. Tunable wavelength hyper-Rayleigh scattering (HRS) measurements were performed on this prototypical octupolar molecule in the broad fundamental wavelength range of 620−1580 nm, showing significant shortcomings of the commonly used $\beta$ dispersion models. Three well-separated $\beta$ resonances involving the lowest-energy state and several higher excited states are clearly observed, including a significant contribution from a *nominally* one-photon forbidden transition. The experimental results for second-harmonic wavelengths above 330 nm are successfully modeled by means of a vibronically coupled essential-state description for octupolar chromophores, developed by Terenziani et al. (*J. Phys. Chem. B* **2008**, *112*, 5079), which takes into account polar solvation effects. The relative intensities of the various resonances, including the one below 330 nm, are also quantified by quantum chemical calculations. Furthermore, interesting effects of inhomogeneous broadening due to polar solvation of the two-dimensional chromophore are recognized in both linear and nonlinear spectra, allowing us to quantitatively address the long-standing problem of the band shape of the linear absorption spectrum of CV. This clearly demonstrates that extensive wavelength-dependent HRS measurements, as presented in this work, are essential to the characterization and design of NLO materials and represent a powerful tool to gain valuable information on molecular excitations and environmental effects in general.

## Introduction

Organic second-order nonlinear optical (NLO) materials have a wide range of potential applications: for example, in optical telecommunication networks as ultrafast photonic switches and electro-optic modulators, and also as optical frequency converters.[1,2] A high second-order NLO response at the molecular level, expressed by the first hyperpolarizability $\beta$, is achieved in organic molecules consisting of extended conjugated chains, noncentrosymmetrically substituted with electron donor (D) and acceptor (A) groups.[1,3,4] This is generally implemented in one-dimensional dipolar molecules, but molecules with octupolar symmetry are even more promising:[5−7] they have comparable or even better NLO properties[8,9] than dipolar molecules, and since octupolar molecules do not possess a permanent dipole moment, they more easily form noncentrosymmetric bulk materials as required to obtain a large macroscopic second-order

[†] University of Antwerp.
[‡] Università di Parma.
[§] University of Mons.

(1) Prasad, P. N.; Williams, D. J., *Introduction to Nonlinear Optical Effects in Molecules and Polymers*; John Wiley: New York, 1991; p 307.
(2) (a) Zyss, J. *Molecular Nonlinear Optics: Materials, Physics, and Devices*; Academic Press: San Diego, CA, 1994; p 512. (b) Shi, Y. Q.; Lin, W. P.; Olson, D. J.; Bechtel, J. H.; Zhang, H.; Steier, W. H.; Zhang, C.; Dalton, L. R. *Appl. Phys. Lett.* **2000**, *77*, 1–3. (c) Chang, C. C.; Chen, C. P.; Chou, C. C.; Kuo, W. J.; Jeng, R. J. *J. Macromol. Sci., Polym. Rev.* **2005**, *C45*, 125–170. (d) Dalton, L. R.; Harper, A.; Ren, A.; Wang, F.; Todorova, G.; Chen, J.; Zhang, C.; Lee, M. *Ind. Eng. Chem. Res.* **1999**, *38*, 8–33.
(3) Chemla, D. S.; Zyss, J., *Nonlinear Optical Properties of Organic Molecules and Crystals*; Academic Press: Orlando, FL, 1987; Vol. 1, p 482.
(4) Goovaerts, E.; Wenseleers, W.; Garcia, M. H.; Cross, G. H. Design and Characterization of Organic and Organometallic Molecules for Second Order Nonlinear Optics. In *Nonlinear Optical Materials*; Nalwa, H. S., Ed.; Academic Press: San Diego, CA, 2001; Vol. 9, pp 127−191.
(5) Zyss, J. *J. Chem. Phys.* **1993**, *98*, 6583–6599.
(6) Zyss, J.; Ledoux, I. *Chem. Rev.* **1994**, *94*, 77–105.
(7) Verbiest, T.; Clays, K.; Samyn, C.; Wolff, J.; Reinhoudt, D.; Persoons, A. *J. Am. Chem. Soc.* **1994**, *116*, 9320–9323.
(8) Joffre, M.; Yaron, D.; Silbey, R. J.; Zyss, J. *J. Chem. Phys.* **1992**, *97*, 5607–5615.
(9) Alcaraz, G.; Euzenat, L.; Mongin, O.; Katan, C.; Ledoux, I.; Zyss, J.; Blanchard-Desce, M.; Vaultier, M. *Chem. Commun.* **2003**, 2766–2767.

***Scheme 1.*** Four Different Resonance Structures of Crystal Violet: Monopolar State $\varphi_0$ and Three Degenerate Dipolar States $\varphi_{1-3}$

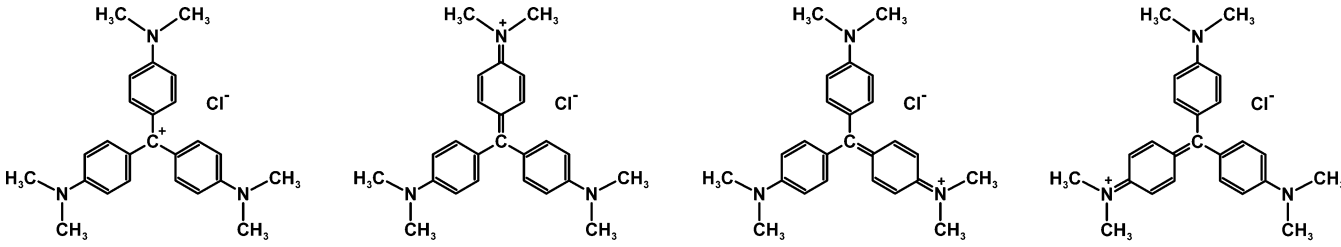

$\varphi_0$ $\varphi_1$ $\varphi_2$ $\varphi_3$

NLO response,[10] in contrast to dipolar push−pull systems that tend to align in a pairwise antiparallel way.

However, due to their two-dimensional character, octupolar molecules have a far more complex electronic structure than dipolar ones,[6,11,12] complicating the interpretation of the experimental NLO results. For further optimization of the first hyperpolarizability $\beta$ of octupolar molecules, it is important to understand the origin of their NLO response, identifying the contributions from different excited states. Furthermore, to enable the comparison of $\beta$ values between different molecules characterized by different resonance frequencies and to assess the potential of an octupolar molecule for applications, it is important to understand the dispersion of $\beta$ in order to be able to extrapolate $\beta$ to technologically relevant frequencies and to the static limit $\beta_0$. In this work, the dispersion of the molecular first hyperpolarizability $\beta$ of the octupolar molecule crystal violet (tris[*p*-(dimethylamino)phenyl]methyl chloride, CV; see Scheme 1) is measured in detail by means of hyper-Rayleigh scattering (HRS)[13,14] and modeled theoretically by use of both essential-state models and quantum chemical approaches. The HRS technique,[13,14] which can be briefly described as incoherent second-harmonic light scattering in solution, does not require any preferential alignment of the molecules, which makes it applicable to nondipolar molecules,[6,7,15−17] in contrast to the formerly often used electric field induced second-harmonic generation (EFISHG) technique.[18]

CV is arguably one of the most prototypical octupolar chromophores and is very well-known for its optical nonlinearity.[12,17,19−22] Nevertheless, as with most organic molecules (including all octupolar molecules studied so far), NLO measurements reported to date have been limited to one[23] or two[20,22] wavelengths,[24] yielding no information on the shape of the $\beta$ resonance spectrum. This molecule is chosen here as an interesting model system because of its high symmetry, its high first hyperpolarizability (in spite of its small size), and its sharp, well-isolated absorption bands. It can be viewed as a superposition of three dipolar molecules rotated over an angle of 0°, 120° and 240°, and the electronic properties can therefore be described by three coupled intramolecular charge transfers (ICT) from the electron-donating dimethylamino groups at the periphery to the central positively charged carbon atom, through the phenylene rings[6,12,16] (see Scheme 1). Both from crystallographic studies[25] and from intermediate neglect of differential overlap (INDO) molecular orbital calculations on the isolated molecule,[26] the equilibrium geometry of CV was found to be that of a three-bladed propeller formed by an out-of-plane rotation of the three dipolarlike arms around the bond connecting the central carbon atom to the phenylene rings. In spite of the large conformational freedom in solution, this octupolar symmetry was also confirmed by means of polarized HRS measurements,[22] although more elaborate measurements using also elliptically polarized light showed significant deviations from the ideal $D_3$ symmetry, indicative of symmetry breaking through solvent interactions.[27]

Here, the shape of the $\beta$ resonances is determined experimentally and described in detail by means of the essential-state model for octupolar molecules developed by Terenziani et al.,[28] which includes coupling of electrons to molecular vibrations as well as solvation effects. Subsequently, in order to understand the origin of the multiple electronic resonances to $\beta$, electronic structure calculations are performed at a semiempirical correlated quantum-chemical level.

## Materials and Methods

The dispersion of the molecular first hyperpolarizability $\beta$ of crystal violet (CV, Sigma, ACS reagent, 91.7%) is determined by the hyper-Rayleigh scattering (HRS) technique,[13,14] making use of our highly sensitive and broadly tunable HRS setup described in


(10) Le Floc'h, V.; Brasselet, S.; Zyss, J.; Cho, B. R.; Lee, S. H.; Jeon, S. J.; Cho, M.; Min, K. S.; Suh, M. P. *Adv. Mater.* **2005**, *17*, 196–200.
(11) Vance, F. W.; Hupp, J. T. *J. Am. Chem. Soc.* **1999**, *121*, 4047–4053.
(12) Beljonne, D.; Wenseleers, W.; Zojer, E.; Shuai, Z. G.; Vogel, H.; Pond, S. J. K.; Perry, J. W.; Marder, S. R.; Bredas, J. L. *Adv. Funct. Mater.* **2002**, *12*, 631–641.
(13) Terhune, R. W.; Maker, P. D.; Savage, C. M. *Phys. Rev. Lett.* **1965**, *14*, 681–684.
(14) Clays, K.; Persoons, A. *Phys. Rev. Lett.* **1991**, *66*, 2980–2983.
(15) Zyss, J.; Dhenaut, C.; Chauvan, T.; Ledoux, I. *Chem. Phys. Lett.* **1993**, *206*, 409–414.
(16) Zyss, J.; Van, T. C.; Dhenaut, C.; Ledoux, I. *Chem. Phys.* **1993**, *177*, 281–296.
(17) Olbrechts, G.; Strobbe, R.; Clays, K.; Persoons, A. *Rev. Sci. Instrum.* **1998**, *69*, 2233–2241.
(18) (a) Levine, B. F.; Bethea, C. G. *Appl. Phys. Lett.* **1974**, *24*, 445–447. (b) Singer, K. D.; Garito, A. F. *J. Chem. Phys.* **1981**, *75*, 3572–3580. (c) Oudar, J. L.; Chemla, D. S.; Batifol, E. *J. Chem. Phys.* **1977**, *67*, 1626–1635.
(19) Chui, T. W.; Wong, K. Y. *J. Chem. Phys.* **1998**, *109*, 1391–1396.
(20) Clays, K.; Persoons, A. *Rev. Sci. Instrum.* **1994**, *65*, 2190–2194.
(21) (a) Yaliraki, S. N.; Silbey, R. J. *J. Chem. Phys.* **1999**, *111*, 1561–1568. (b) Lee, Y. K.; Jeon, S. J.; Cho, M. H. *J. Am. Chem. Soc.* **1998**, *120*, 10921–10927.
(22) Rao, Y.; Guo, X. M.; Tao, Y. S.; Wang, H. F. *J. Phys. Chem. A* **2004**, *108*, 7977–7982.
(23) Verbiest, T.; Hendrickx, E.; Persoons, A.; Clays, K. *Proc. SPIE—Int. Soc. Opt. Eng.* **1992**, *1775*, 206–212.
(24) Available measurements in literature are moreover obtained with various setups in different circumstances, some of which[20,23] are known to be erroneous due to 2PA-induced fluorescence and unreliable referencing.[30]
(25) Stora, C. C. R. *Acad. Sci., Ser. 2* **1958**, *246*, 1693.
(26) Lueck, H. B.; McHale, J. L.; Edwards, W. D. *J. Am. Chem. Soc.* **1992**, *114*, 2342–2348.
(27) Ostroverkhov, V.; Petschek, R. G.; Singer, K. D.; Sukhomlinova, L.; Twieg, R. J.; Wang, S. X.; Chien, L. C. *J. Opt. Soc. Am. B* **2000**, *17*, 1531–1542.
(28) Terenziani, F.; Sissa, C.; Painelli, A. *J. Phys. Chem. B* **2008**, *112*, 5079–5087.

ref 29. Briefly, the laser system is based on a Ti:sapphire regenerative amplifier (Spectra-Physics Spitfire), which is pumping an optical parametric amplifier (Spectra-Physics OPA-800CP), allowing the output (pulse width 2 ps, repetition rate 1.5 kHz) to be tuned in the wavelength range from 300 nm to 3 $\mu$m. A narrow spectral window around the second-harmonic wavelength is detected in parallel by means of an intensified charge-coupled device (CCD) coupled to a spectrograph. Only for the measurements in methanol in the fundamental wavelength range of 1060−1200 nm was the formerly used serial detection setup applied, where the scattered second-harmonic light is analyzed with a monochromator and detected with a Peltier-cooled photomultiplier tube (PMT) as described in ref 4. In both setups, the spectral analysis enables complete correction for broadband multiphoton absorption-induced fluorescence (MPF).[4,13,22,30]

Two different solvents (chloroform and methanol) were used, allowing the solvent effect to be probed. The covered wavelength range is limited at the short-wavelength side for chloroform by photochemical decomposition of CV and at the long-wavelength side (≥1400 nm) for methanol by the infrared (IR) transparency of the solvent. For excitation wavelengths shorter than 800 nm, severe decomposition (observed through a decrease of the lowest-energy absorption band) in the focused laser beam took place in chloroform, while in methanol the decomposition became only significant (i.e., more than 10% during a series of measurements) at 620 nm. To reduce the effect of this decomposition on the HRS signal, the molecules in the laser focus were continuously refreshed by stirring the solution during the measurement.[29]

Due to the high sensitivity of the setup, the pure solvents, which themselves have a smooth and monotonous dispersion of $\beta$, could be used as internal calibration over the entire wavelength range. Moreover, the HRS results presented here are corrected for this $\beta$ dispersion of the pure solvent by means of the calibration parameters reported in ref 29 (in turn based on the effective $|\beta_{zzz}|$ value of 0.49 $\times$ $10^{-30}$ esu for chloroform,[31] determined with the EFISHG technique at 1064 nm).

The first hyperpolarizabilities reported in this work are $\beta_{HRS}$ values, given by

$$\beta_{HRS} = \sqrt{\langle \beta_{ZZZ}^2 \rangle + \langle \beta_{XZZ}^2 \rangle} \quad (1)$$

where capital indices stand for Cartesian components in the laboratory reference frame and $\langle \beta_{III}^2 \rangle$ stands for the orientational average of the square of the appropriate $\beta$ tensor component, which can be expressed as a combination of the $\beta_{ijk}$ tensor elements,[32] where lowercase indices indicate Cartesian components in the molecular reference frame. Depending on symmetry, some of the $\beta_{ijk}$ tensor elements are zero, and specific relationships connect some of the tensor elements, which simplifies the expression for $\beta_{HRS}$. Strictly speaking, CV belongs to the $D_3$ space group (propeller shape), so that out-of-plane $\beta_{ijk}$ components may be nonzero (i.e., $\beta_{yzz}$ and $\beta_{xyz}$ if $xy$ is defined to be the mean molecular plane).[6] However, for CV these out-of-plane components are generally assumed to be negligible with respect to the in-plane ones.[6,7,16,17,19,22] The theoretical results in the present work are also consistent with this assumption (see section Quantum-Chemical Calculations). In this approximation, CV can be considered as a trigonal planar molecule lying in the $xy$-plane. If $D_{3h}$ symmetry is assumed, the only nonzero components of the $\beta$ tensor are $\beta_{xxx} = -\beta_{xyy} = -\beta_{yxy} = -\beta_{yyx}$ (with the $x$-axis oriented along one of the three molecular arms),[7,16] so that just a single independent parameter is left. In these conditions the observable $\beta_{HRS}$ is proportional to the molecular $|\beta_{xxx}|$ component:[16] $\beta_{HRS}^{D_{3h}} = (8/21)^{1/2}|\beta_{xxx}|$. The pure solvent is used as internal calibration and is treated as if it were a dipolar molecule with an effective $\beta_{xxx}$ value (having no physical meaning other than an effective calibration constant) for HRS as discussed in ref 29, resulting in the following equation for the $\beta_{HRS}$ of CV:[4]

$$\beta_{HRS} = \sqrt{\frac{N_{solvent}}{N_{CV}} \frac{S_{solution}^{(2\omega)} - S_{solvent}^{(2\omega)}}{S_{solvent}^{(2\omega)}}} \sqrt{\frac{6}{35}} \left| \beta_{xxx}^{eff,solvent} \right| \quad (2)$$

In this expression, $N$ stands for number density and $S^{(2\omega)}$ for the HRS signal. Reported results for $\beta$ are expressed in the B* convention as defined by Willetts et al.[33]

Although CV is commonly considered a nonfluorescent molecule, we observed strong MPF in many of our HRS experiments, which could in each case be eliminated completely thanks to the spectral measurement around the second-harmonic wavelength. In the fundamental wavelength region from 700 to 810 nm, direct two-photon fluorescence from the second excited state was observed for CV in methanol, as also reported by Rao and co-workers.[22] The relative fluorescence contribution was strongest in the HRS measurement at 760 nm, that is, about 15 times the HRS signal when integrated over the 4 nm wide central part of the detected spectral range, and even 950 times stronger when the entire $S_2 \rightarrow S_0$ emission spectrum [full width at half-maximum (fwhm) ∼50 nm] is taken into account. Also, the measurements in the fundamental wavelength intervals 1100−1300 and 620−660 nm showed significant fluorescence (about 7 times the HRS signal at 1220 nm as well as at 620 nm, based on the central intervals of 6 and 3 nm, respectively). This once more clearly illustrates the importance of systematic and complete correction for MPF, even when the solute is considered to be virtually nonfluorescent.[4,13,22,30] Such a correction is possible only by spectral analysis of the collected light, as applied here. Indeed, the alternative techniques based on the time difference between HRS and MPF (e.g., by high-frequency demodulation[17]) are not suitable to correct HRS measurements, not even for CV, not only because the fluorescence/HRS intensity ratio is too large at some wavelengths (despite its exceptionally low fluorescence quantum efficiency, ∼0.01% in methanol at room temperature) but also because the fluorescence is known to exhibit a fast (picosecond) decay time,[34] way beyond the range of the electronic demodulation method. Note that CV has nevertheless (inappropriately) been used as a nonfluorescent benchmark molecule to validate the demodulation-based MPF suppression technique.[17] In our setup, which makes use of 2 ps pulses,[29] the HRS signal has a narrow spectral width and can therefore be clearly distinguished from the strong but broad multiphoton fluorescence background. This is in contrast to the setup employed by Rao et al.,[22] where a femtosecond laser source (pulse width 80 fs) is applied, resulting in a larger spectral width of the HRS signal. Indeed, in spite of the great care with which the state-of-the-art work in ref 22 was clearly performed, they reported to be unable to perform HRS measurements on CV (in methanol) at fundamental wavelengths shorter than 800 nm because the signal was too weak compared to the strong background of direct emission from the second excited state.[22]

In the HRS measurements at short fundamental wavelengths (≤830 nm), we observed a weak hyper-Raman signal for CV (roughly at ∼440 $cm^{-1}$; for longer laser wavelengths this Stokes

(29) Campo, J.; Desmet, F.; Wenseleers, W.; Goovaerts, E. *Opt. Express* **2009**, *17*, 4587–4604.
(30) (a) Flipse, M. C.; Dejonge, R.; Woudenberg, R. H.; Marsman, A. W.; Vanwalree, C. A.; Jenneskens, L. W. *Chem. Phys. Lett.* **1995**, *245*, 297–303. (b) Noordman, O. F. J.; van Hulst, N. F. *Chem. Phys. Lett.* **1996**, *253*, 145–150. (c) Stadler, S.; Bourhill, G.; Brauchle, C. *J. Phys. Chem.* **1996**, *100*, 6927–6934. (d) Morrison, I. D.; Denning, R. G.; Laidlaw, W. M.; Stammers, M. A. *Rev. Sci. Instrum.* **1996**, *67*, 1445–1453. (e) Song, N. W.; Kang, T. I.; Jeoung, S. C.; Jeon, S. J.; Cho, B. R.; Kim, D. *Chem. Phys. Lett.* **1996**, *261*, 307–312.
(31) Kajzar, F.; Ledoux, I.; Zyss, J. *Phys. Rev. A* **1987**, *36*, 2210–2219.
(32) (a) Cyvin, S. J.; Rauch, J. E.; Decius, J. C. *J. Chem. Phys.* **1965**, *43*, 4083–4095. (b) Bersohn, R.; Pao, Y. H.; Frisch, H. L. *J. Chem. Phys.* **1966**, *45*, 3184–3198.
(33) Willetts, A.; Rice, J. E.; Burland, D. M.; Shelton, D. P. *J. Chem. Phys.* **1992**, *97*, 7590–7599.
(34) Doust, T. *Chem. Phys. Lett.* **1983**, *96*, 522–525.

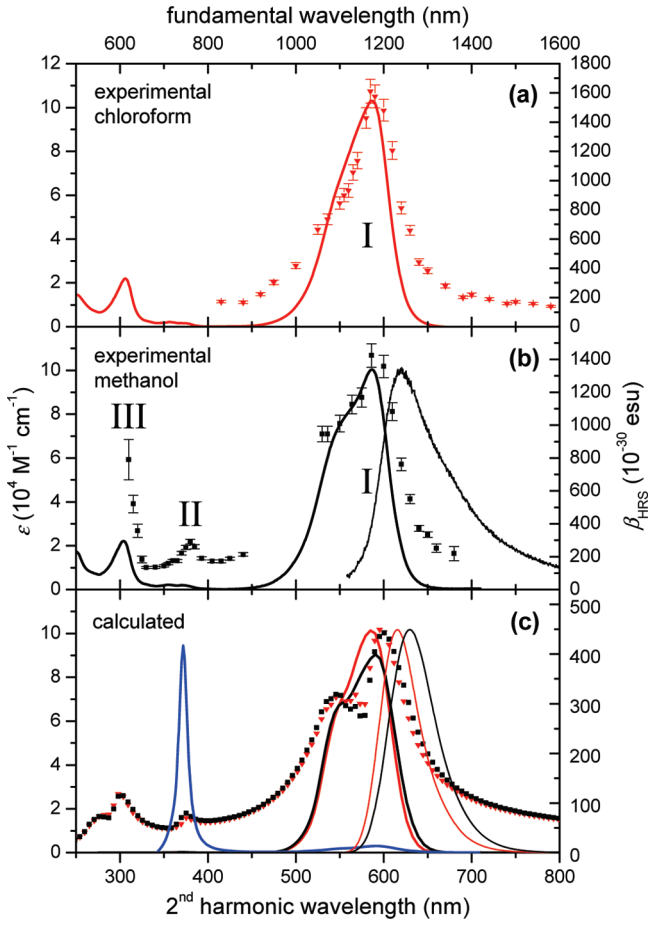


***Figure 1.*** (a) Experimental HRS data (red triangles) and linear absorption spectrum (thick line) of CV in chloroform. (b) Experimental HRS data (black squares), linear absorption spectrum (thick line), and normalized experimental fluorescence spectrum (thin line) of CV in methanol. (c) Calculated (essential-state model) $\beta_{HRS}$ values (symbols), linear absorption spectrum (thick line), and normalized fluorescence spectrum (thin line) of CV in chloroform (red, $\varepsilon_{or} = 0.20$ eV) and methanol (black, $\varepsilon_{or} = 0.27$ eV), making use of the molecular parameters in Table 1, shown together with the calculated two-photon absorption spectrum of CV in methanol (blue line, normalized, peak value = $3933 \times 10^{-50}$ cm$^4$·s·photon$^{-1}$). The linear absorption and emission spectra are plotted versus the second-harmonic wavelength in all panels. I, II, and III indicate the three observed $\beta$ resonance regions as referred to in the text.

shift is outside the measured spectral range). Furthermore, beyond the wavelength range normally detected for the HRS measurements (not shown), several other modes were found (at ~1190, 1400, 1500, and 1600 cm$^{-1}$), the strongest one being at ~1400 cm$^{-1}$ as can be expected for a conjugated ICT molecule. This is in agreement with the observation made by Rao et al.,[22] who reported a hyper-Raman scattering signal of CV at 1415 ± 25 cm$^{-1}$, attributed to the phenyl groups in the CV molecule, as well as with the more resolved spectra reported in ref 35.

The concentrations used ($10^{-6}$–$10^{-4}$ M in chloroform and $10^{-6}$–$10^{-5}$ M in methanol) were chosen to keep the absorption of the second-harmonic wavelength well below 10%, so that reabsorption could be accurately corrected for. The experimental error on $\beta$ (not including the systematic error on the reference standard value) is estimated to be ±5%, increasing up to ±10% and even ±20% for a few wavelengths (see Figure 1) at which additional complications occur (decomposition or significant solvent absorption at the fundamental wavelength).

***Table 1.*** Molecular Model Parameters for CV

| $z$, eV | $2^{1/2}t$, eV | $\omega_v$, eV | $E_v$, eV | $\mu_0$, D | Γ, eV |
|---|---|---|---|---|---|
| 0.53 | 0.91 | 0.13 | 0.08 | 18.5 | 0.05 |

Absorption spectra at low temperatures were recorded on a Perkin-Elmer Lambda 650 spectrophotometer used in single-channel configuration, equipped with an Oxford Instruments OptistatDN cryostat providing a controlled low-temperature exchange gas environment for the sample (inside a quartz cuvette for cryogenics). For each temperature, data were collected for the sample (CV in methanol) and the pure solvent, the latter being used as the reference.

Fluorescence measurements were performed by means of a spectrograph (Acton Spectrapro 2300i) with liquid nitrogen-cooled deep depletion CCD detector (Princeton Instruments, Spec-10 400BR) using the 528.7 nm output from an $Ar^+$ laser (Spectra-Physics 2020) for excitation. The spectral efficiency of the spectrograph and detector were calibrated by use of a halogen lamp, the emission spectrum of which was approximated by a blackbody spectrum.

## Results and Discussion

**Hyper-Rayleigh Scattering Data.** The experimental wavelength-dependent hyper-Rayleigh scattering (HRS) results obtained for crystal violet (CV) are shown in Figure 1a,b together with linear absorption and fluorescence data, measured in chloroform and methanol, respectively. Several well-separated regions with $\beta$ resonances are clearly revealed, and these are labeled I−III to facilitate the discussion below.

The extensive experimental data set depicted in Figure 1a,b holds a wealth of information about $\beta$ (the wavelength position as well as the shape and the relative amplitudes of the various resonances) and will therefore be a critical test of the $\beta$ dispersion models applied below. To the best of our knowledge, this is the first time that contributions to the first hyperpolarizability originating from multiple electronic transitions (among which is a *quasi* one-photon forbidden transition, see below) are directly resolved by HRS. In a different way, Shoute et al.[36] have demonstrated that the HRS resonance profile of a dipolar molecule, when combined with information obtained from a remarkable set of hyper-Raman excitation profiles for several specific vibrational modes, can be disentangled into contributions from separate transitions. The only other report known to us of second-order NLO resonance effects arising from several higher-energy transitions is the early experimental work by Heinz et al.[37] (later studied theoretically[38]), in which coherent second-harmonic generation (SHG) measurements were performed on a monolayer of rhodamine dyes, clearly revealing one- and two-photon resonances involving three different electronic states. The importance of multiple excited states in the NLO response of organic molecules has also been demonstrated for the case of two-photon absorption (2PA),[39] a third-order but by definition fully resonant process.

(35) Kelley, A. M.; Shoute, L. C. T.; Blanchard-Desce, M.; Bartholomew, G. P.; Bazan, G. C. *Mol. Phys.* **2006**, *104*, 1239–1247.
(36) Shoute, L. C. T.; Blanchard-Desce, M.; Kelley, A. M. *J. Phys. Chem. A* **2005**, *109*, 10503–10511.
(37) Heinz, T. F.; Chen, C. K.; Ricard, D.; Shen, Y. R. *Phys. Rev. Lett.* **1982**, *48*, 478–481.
(38) Lin, S. H.; Alden, R. G.; Villaeys, A. A.; Pflumio, V. *Phys. Rev. A* **1993**, *48*, 3137–3151.
(39) Zojer, E.; Wenseleers, W.; Pacher, P.; Barlow, S.; Halik, M.; Grasso, C.; Perry, J. W.; Marder, S. R.; Bredas, J. L. *J. Phys. Chem. B* **2004**, *108*, 8641–8646.

The various resonance contributions to $\beta$ can be understood in terms of the general sum-over-states (SOS) expression,[40] which is based on a perturbative treatment of the interaction between light and matter:[33]

$$\beta_{ijk}(-2\omega;\omega,\omega) = \frac{1}{6\hbar^2}\sum_{m,n}\left\langle \frac{\langle g|\mu_i|m\rangle\langle m|\bar{\mu}_j|n\rangle\langle n|\mu_k|g\rangle}{(\Omega_{mg}-2\omega)(\Omega_{ng}-\omega)} + \frac{\langle g|\mu_i|m\rangle\langle m|\bar{\mu}_k|n\rangle\langle n|\mu_j|g\rangle}{(\Omega_{mg}-2\omega)(\Omega_{ng}-\omega)} + \frac{\langle g|\mu_j|m\rangle\langle m|\bar{\mu}_i|n\rangle\langle n|\mu_k|g\rangle}{(\Omega^*_{mg}+\omega)(\Omega_{ng}-\omega)} + \frac{\langle g|\mu_k|m\rangle\langle m|\bar{\mu}_i|n\rangle\langle n|\mu_j|g\rangle}{(\Omega^*_{mg}+\omega)(\Omega_{ng}-\omega)} + \frac{\langle g|\mu_k|m\rangle\langle m|\bar{\mu}_j|n\rangle\langle n|\mu_i|g\rangle}{(\Omega^*_{mg}+\omega)(\Omega^*_{ng}+2\omega)} + \frac{\langle g|\mu_j|m\rangle\langle m|\bar{\mu}_k|n\rangle\langle n|\mu_i|g\rangle}{(\Omega^*_{mg}+\omega)(\Omega^*_{ng}+2\omega)} \right\rangle \quad (3)$$

In this expression, $\omega$ stands for the laser frequency and $\Omega_{mg} = \omega_{mg} - i\gamma_{mg}$, with $\omega_{mg}$ corresponding to the excitation energy of state $m$ and with $\gamma_{mg}$ representing an ad hoc homogeneous damping parameter. The $m$ and $n$ indices run over all excited states, so that the summation includes nondegenerate ($m \neq n$) as well as degenerate ($m = n$) level terms. The relative weight of each term is determined by the transition dipole moments ($\mu_i$ is the dipole moment operator in the $i$ direction) between the different levels and, in the case of a two-level term, by the difference between the dipole moment in the ground and excited states: $\langle m|\bar{\mu}|n\rangle = \langle m|\mu|n\rangle - \langle g|\mu|g\rangle\delta_{mn}$. The simplest relevant description of the dispersion of $\beta$ for octupolar molecules, as proposed by Joffre et al.,[8] consists of a two-level (three-state) model that takes into account only the ground and the doubly degenerate first excited state:

$$\beta_{xxx}(-2\omega;\omega,\omega) = \beta_{0,xxx}\frac{\omega_{eg}^4}{(\omega_{eg}^2-\omega^2)(\omega_{eg}^2-4\omega^2)} = \frac{3e^2 f_{osc}\mu_{12}}{2\hbar m\omega_{eg}^3}\frac{\omega_{eg}^4}{(\omega_{eg}^2-\omega^2)(\omega_{eg}^2-4\omega^2)} \quad (4)$$

where $\omega_{eg}$ corresponds to the energy of the electronic transition and $\omega$ is the laser frequency, $\beta_{0,xxx}$ is the static value of the first hyperpolarizability, $f_{osc}$ is the oscillator strength of the transition, and $\mu_{12}$ is the transition dipole moment between the two degenerate excited states. The above expression (eq 4) (thus in general also the degenerate level contributions in eq 3) is strictly analogous to the two-level model (TLM) expression for dipolar molecules,[41] the only difference being that here the dipole moment difference between the ground and excited states, $\Delta\mu$, is replaced by the transition dipole between the two degenerate excited states, $\mu_{12}$. While eq 4 is a useful starting point, we will improve on it in several respects. First of all, just as with the TLM relevant to dipolar molecules, eq 4 does not account for any vibrational or environmental broadening of the electronic transitions[36,42−44] and hence does not properly describe the $\beta$ dispersion near resonance. Moreover, the minimal model for the electronic structure of octupolar molecules considers at least four states (corresponding to the main charge-resonant forms; see Scheme 1), and the experimental results presented here indeed show the need to extend the description to more than just two levels (or three states).

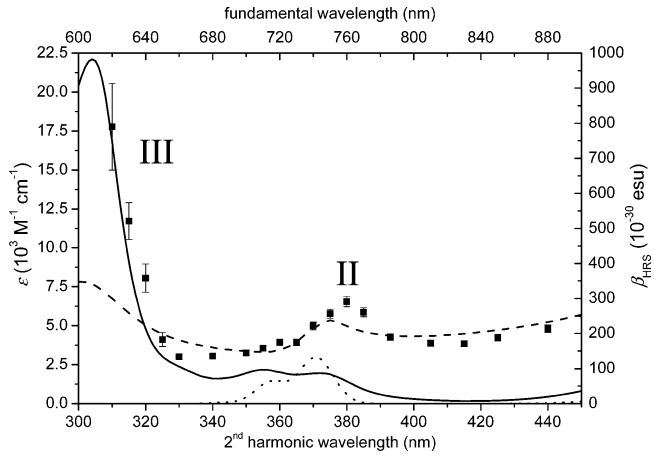


***Figure 2.*** Detailed view of (part of) the short-wavelength data of CV in methanol (shown in Figure 1b,c): experimental (symbols) and calculated essential-state (dashed line, magnified 3 times) HRS data and experimental (solid line) and calculated (dotted line, magnified 10 times) linear absorption spectra. The absorption spectra are plotted versus the second-harmonic wavelength, and II and III indicate the observed $\beta$ resonance regions as referred to in the text.

In particular, the absorption spectrum of CV exhibits a very strong band at about 590 nm with a partly resolved shoulder at the high-energy side, two very weak overlapping bands at about 374 and 354 nm, and another electronic transition at about 304 nm (see Figure 1). The lowest-energy band represents the main transition in the absorption spectrum and is expected to give the largest contribution to $\beta$. Indeed, the two-photon resonance enhancement from this level (I) is huge, resulting in a more than 10 times higher $\beta$ at resonance compared to the off-resonant value at 1580 nm in chloroform (see Figure 1a). Note that the high-energy shoulder is also visible in the HRS data (although less pronounced than calculated, at least in chloroform) and that it is generally more pronounced in the spectra collected in methanol (see Figure 1b). Very detailed HRS measurements (5 nm steps in second-harmonic wavelength) were performed from 620 to 880 nm (in methanol, for photochemical stability; see Figure 2 for a magnification of these data) to unambiguously identify another weak two-photon resonance, associated with the very weak transition observed in the absorption spectrum at about 374 nm (II).

Also in this second resonance region, a short-wavelength shoulder is observed in HRS (at about 360 nm), most probably associated with the weak linear absorption band at about 354 nm. The two-photon resonance with the second excited state (II) is particularly intriguing: in fact, this state is one-photon forbidden for $D_3$ symmetry and thus should not contribute to $\beta$.[41] On the other hand, in the same region a weak band is visible in the absorption spectrum, albeit with an almost 2 orders of magnitude lower extinction coefficient than the dominant lowest-energy band, suggesting the activation of this transition either due to vibronic effects or due to the relaxation of the molecular geometry to a lower symmetry. Indeed, direct emission from this state was observed in ref 22 under one-photon excitation by means of ~365 nm laser light, and this state was found to have a very large 2PA intensity.[12,22] Note that, in line with the

(40) Orr, B. J.; Ward, J. F. *Mol. Phys.* **1971**, *20*, 513–526.
(41) Oudar, J. L.; Chemla, D. S. *J. Chem. Phys.* **1977**, *66*, 2664–2668.
(42) Vance, F. W.; Karki, L.; Reigle, J. K.; Hupp, J. T.; Ratner, M. A. *J. Phys. Chem. A* **1998**, *102*, 8320–8324. Painelli, A.; Terenziani, F. *Synth. Met.* **2000**, *109*, 229–233. Painelli, A.; Terenziani, F. *Synth. Met.* **2001**, *124*, 171–173. Kelley, A. M. *J. Opt. Soc. Am. B* **2002**, *19*, 1890–1900. Moran, A. M.; Egolf, D. S.; Blanchard-Desce, M.; Kelley, A. M. *J. Chem. Phys.* **2002**, *116*, 2542–2555. Shoute, L. C. T.; Bartholomew, G. P.; Bazan, G. C.; Kelley, A. M. *J. Chem. Phys.* **2005**, *122*, 184508.
(43) Painelli, A.; Terenziani, F. *Synth. Met.* **2001**, *116*, 135–138.
(44) Campo, J.; Wenseleers, W.; Goovaerts, E.; Szablewski, M.; Cross, G. *J. Phys. Chem. C* **2008**, *112*, 287–296.

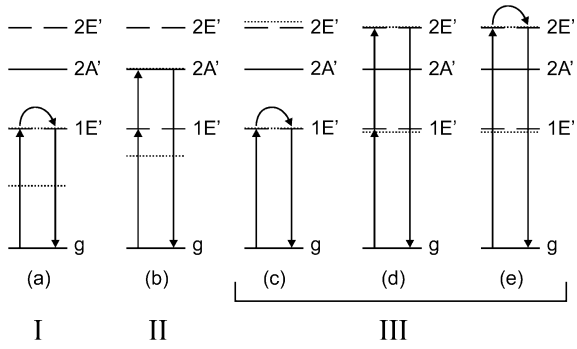


***Figure 3.*** Energy level diagrams representing the terms in the sum-over-states (SOS) expression (eq 3) for $\beta$, which are important in the description of the resonances observed for CV. Dotted lines indicate the laser and second-harmonic energies for the corresponding resonance regions.

observations for 2PA,[12,22] resonance II occurs (mostly) at about 380 nm and only to a much lesser extent at the linear absorption maximum at 354 nm. Finally, the third resonance (III) at a second-harmonic wavelength of about 300 nm is also special, as a virtually exact double resonance occurs here. The one-photon resonance with the first excited state overlaps with the two-photon resonance with the higher-energy state observed in the linear absorption spectrum at ~304 nm, resulting in a sharp increase of $\beta$. The energy level diagrams representing the main resonance terms in the SOS expression (eq 3) to which the resonances I−III can be attributed are shown in Figure 3.

In this figure the electronic state at about 304 nm (2E′) is depicted for simplicity as the third electronic level although it is not really the third state, because more states are expected in this region that are very weak or forbidden in one-photon absorption and are found to give a negligible contribution to $\beta$. On the basis of this schematic representation, the various $\beta$ resonances can be interpreted qualitatively. For the first resonance (I), the most obvious description is of course a degenerate level term with the dominant lowest-energy transition (diagram a in Figure 3). From energy level diagram b, which describes the second resonance (II), it becomes clear why the virtually one-photon forbidden excited state 2A′ is still leading to a significant $\beta$ resonance. Although the transition dipole from the ground to the second excited state is small, all other molecular parameters that are important for $\beta$ are very favorable. Indeed, both the transition dipole from g to 1E′ and from 1E′ to 2A′ are known to be large,[12] and term b is quite close to double resonance. Furthermore, relative to resonance I, resonance II is more important in $\beta$ than in linear absorption (see Figure 1b) but less than in 2PA.[12] This can be understood from the small transition dipole moment between the ground state g and 2A′, which is associated with the downward arrow in diagram b, not occurring in 2PA. The fact that the contribution of this *quasi*-forbidden one-photon transition is not negligible is very promising for analogous molecules with lower symmetry, for which this transition becomes allowed. For region III a double-resonance-type term (diagram d in Figure 3) can be important, as the resonance factor is huge (two small factors in the denominator) and at least two of the transition dipoles are significant (g to 2E′) or even large (g to 1E′). Of course, also the degenerate level terms for 1E′ (energy level diagram c, in Figure 3, corresponding to the same term as diagram a) and for 2E′ (term e) can contribute to this resonance. In particular, according to expression 3, the degenerate level term for 1E′ (c) gives rise to a one-photon resonance at about 300 nm with 4 times smaller amplitude than the corresponding two-photon resonance I at about 600 nm, and therefore it accounts for only a fraction of the observed amplitude of $\beta$ peak III. Similarly, the near double-resonance term b can contribute to peak III, but this contribution is known from $\beta$ peak II to be relatively small. Finally, a two-photon resonant term reaching 2E′, with 2A′ as the intermediate level (not shown in Figure 3), may also contribute to resonance III. However, this contribution is expected to be much weaker than term d because it is less resonant, the first transition dipole involved is much smaller than for d, and the transition dipole between 2A′ and 2E′ is relatively small as well (see below).

**Modeling Vibronic Coupling and Solvation.** For a detailed description of the optical spectra of CV, including the shape of the resonances, it is necessary to account for coupling between electronic and vibrational degrees of freedom as well as for polar solvation. Therefore, we will extend the vibronically coupled essential-state model, which was recently developed for neutral octupolar chromophores,[28] to the present case of an ionic octupole. Indeed, apart from the presence of a net positive charge, CV belongs to the family of A(-$\pi$-D)$_3$ chromophores and can be described accordingly.[28] The central positively charged carbon atom acts as a strong electron acceptor with respect to the three coplanar peripheral amino groups connected through $\pi$-conjugated bridges. This causes the charge to delocalize, resulting in four resonance structures with planar or almost planar geometry, as depicted in Scheme 1. The corresponding four electronic states $\varphi_{0-3}$ define the minimal (essential) basis set to describe the electronic structure of CV. The lowest-energy state $\varphi_0$ corresponds to the $|N\rangle$ state of neutral octupolar chromophores,[28] and the three degenerate states $\varphi_{1-3}$, where the positive charge is displaced along one of the three molecular branches, play the same role as the zwitterionic states $|Z_1\rangle$, $|Z_2\rangle$, and $|Z_3\rangle$ of neutral octupolar dyes.[28] In principle, the dipole moment of charged species is ill-defined; however, we take advantage of the symmetric nature of CV and expand the charge distribution in terms of monopolar and dipolar charges located in the molecular center. Because the monopole charge is invariant in all basis states, it becomes irrelevant in the subsequent discussion. The dipole vanishes in state $\varphi_0$, while the three degenerate states $\varphi_{1-3}$ have dipole moments of equal length, $\mu_0$, each pointing along one of the three molecular arms.

We define the energy gap between $\varphi_0$ and the degenerate $\varphi_{1-3}$ states as $2z$, while $-2^{1/2}t$ represents the matrix element that mixes $\varphi_0$ with each one of the three degenerate states (see the Supporting Information, eqs S4 and S5). The three arms of the molecule are interchanged by a $C_3$ rotation, so that the three degenerate basis states are conveniently combined into a symmetric wave function $\varphi_+ = (\varphi_1 + \varphi_2 + \varphi_3)/3^{1/2}$, and two degenerate functions of E-symmetry that can be chosen as $1E'_x = (2\varphi_1 - \varphi_2 - \varphi_3)/6^{1/2}$ and $1E'_y = (\varphi_2 - \varphi_3)/2^{1/2}$. The two totally symmetric states $\varphi_0$ and $\varphi_+$ mix up to give the ground state, $g = (1 - \rho)^{1/2}|N\rangle + \rho^{1/2}|Z_+\rangle$, and the highest-energy eigenstate, $2A' = \rho^{1/2}|N\rangle - (1 - \rho)^{1/2}|Z_+\rangle$.[45] These two totally symmetric states are fully defined by a single parameter, $\rho$, which measures the amount of positive charge transferred in the ground state from the central carbon atom toward the three lateral branches. The two degenerate E-symmetry states stay

(45) Note that the term "essential state model" as used in the present work (and in refs 12 and 28) should not be confused with the model of Joffre,[8] which includes only g and 1E′ (the minimum to obtain a nonzero $\beta$). In contrast, the present definition of "essential state model" (g, 1E′, and 2A′) includes 2A′ as well, because it follows automatically from symmetry.

unmixed and are accessible by 1PA. All excited states can be reached by 2PA, but the transition toward the $2A_1$ state largely dominates the 2PA spectrum.[12,22,28]

In order to obtain a detailed description of optical spectra, the essential-state model for the electronic structure must be extended to take into account the coupling between electronic and vibrational degrees of freedom, as well as polar solvation. We follow a strategy that was developed for and successfully applied to linear and nonlinear optical absorption/emission spectra of (neutral) polar,[46] quadrupolar,[47] and octupolar[28] chromophores. In multibranched chromophores, at least one vibrational degree of freedom must be introduced for each molecular arm, to describe the relaxation of the geometry that follows the charge transfer in each arm. Specifically, for octupolar chromophores we introduce three effective harmonic vibrational coordinates $q_1$, $q_2$, and $q_3$ with the same frequency $\omega_v$. Each of the four basis states $\varphi_{0-3}$ is then assigned a harmonic potential energy (hyper)surface (PES) on the three coordinates. Setting the origin of the coordinate axis at the equilibrium for $\varphi_0$, each of the three PES relevant to the $\varphi_{1-3}$ states is displaced along the relevant coordinate $q_{1-3}$ by the same amount $(2E_v)^{1/2}/\omega_v$, where $E_v$ is the vibrational relaxation energy associated with the charge transfer. The three molecular coordinates are conveniently combined to give a symmetric coordinate and two degenerate coordinates of E-symmetry (see the Supporting Information, eq S8). The presence of nontotally symmetric vibrations in octupolar chromophores leads to interesting spectroscopic effects, such as vibronic activation (through the so-called Herzberg−Teller mechanism)[48] of forbidden transitions and symmetry-breaking or localization phenomena, whose manifestation has been recently recognized in the strongly solvatochromic fluorescence observed for quadrupolar and octupolar dyes.[47]

Due to the fairly complex structure of the excited states, it is hard to describe optical spectra of octupolar chromophores in the adiabatic approximation. Therefore we numerically diagonalize the nonadiabatic Hamiltonian that describes the coupled electronic and vibrational problem. The relevant basis is the direct product of the electronic basis (the four states $\varphi_{0-3}$) times the eigenstates of the harmonic oscillators associated with the three effective molecular coordinates. Each harmonic oscillator itself defines an infinite basis set; therefore, we truncate the basis disregarding states with a total number of vibrational quanta (summing up on all three oscillators) larger than $M$. The truncated basis increases as $4M^3/3$ and the relevant Hamiltonian matrix is diagonalized for finite $M$ to get numerically exact nonadiabatic eigenstates. The minimum $M$ required to get convergence depends on the model parameters and on the properties of interest. All results presented here have been obtained with $M = 4$ and have been checked for convergence. The nonadiabatic eigenstates describe both the electronic and vibrational motion and, in the adiabatic limit, converge to the familiar vibronic states (product of an electronic and a vibrational wave function).

Once the nonadiabatic eigenstates are obtained, we can calculate absorption spectra as a sum of all transitions from the ground to the excited nonadiabatic states, assigning to each transition a Gaussian line shape with fixed half width at half-maximum (hwhm) $\Gamma$.[49] Emission spectra can be calculated by summing up all transitions from the emissive state toward lower-energy states, modeling each transition in terms of the same Gaussian function used for the absorption process. The emissive state is identified as the first excited state with a sizable transition dipole moment from the ground state.[28] Finally, the nonlinear coefficients $\beta_{ijk}$ entering the $\beta_{HRS}$ expression (see Supporting Information) can be calculated according to the standard sum-over-states expressions (eq 3), with the sums extended over all nonadiabatic eigenstates. The 2PA spectra are calculated along the same line, adopting the relevant sum-over-states expression.[28]

In the simplest model for polar solvation, the solvent is described as a continuum dielectric medium.[50] Specifically, the polar molecules of the solvent reorient around the solute molecules, generating a reaction field, $F_{or}$, proportional to the solute dipole moment. We assume a planar geometry for CV so that only the two components of the reaction field in the molecular plane, $F_x$ and $F_y$, are relevant. The reaction field enters the molecular Hamiltonian with a term $-\hat{\mu}_x F_x - \hat{\mu}_y F_y$, where $\hat{\mu}_x$ and $\hat{\mu}_y$ are the two components of the molecular dipole moment operator (see the Supporting Information, eq S7). The elastic restoring force for the solvent is $\mu_0^2 F_{or}^2/4\varepsilon_{or}$, where $F_{or}^2 = F_x^2 + F_y^2$ and $\varepsilon_{or}$, the solvation relaxation energy, increases with solvent polarity.[51] The polar component of the reaction field, associated with the orientational motion of the solvent molecules, describes a slow motion with respect to both the electronic and vibrational degrees of freedom. As a consequence, $F_x$ and $F_y$ can be treated as classical variables. Then, in each point of the $F_x$,$F_y$ plane we define the relevant molecular Hamiltonian accounting for the coupled electron and vibrational problem, as described above, and for the interaction with the reaction field. The resulting nonadiabatic Hamiltonian is numerically diagonalized, yielding a set of vibronic eigenstates for each $F_x$,$F_y$ point. Linear and nonlinear spectra are then calculated in each point of the plane as described above. Solution spectra are finally obtained as an incoherent sum of the spectra obtained for each $F_x$,$F_y$ point, each spectrum being weighed according to the relevant Boltzmann distribution. Specifically, for (linear and nonlinear) absorption spectra and for HRS spectra the Boltzmann distribution is built on the basis of the total ground-state energy, while for steady-state fluorescence spectra it is built on the energy of the fluorescent state.[28] Our model not only describes the modulation of the energy of molecular states in polar solvents but also quite naturally accounts for inhomogeneous broadening phenomena related to polar solvation. In a polar solvent, in fact, each solute molecule experiences

(46) (a) Painelli, A.; Terenziani, F. *Chem. Phys. Lett.* **1999**, *312*, 211–220. (b) Painelli, A.; Terenziani, F. *J. Phys. Chem. A* **2000**, *104*, 11041–11048. (c) Terenziani, F.; Painelli, A.; Comoretto, D. *J. Phys. Chem. A* **2000**, *104*, 11049–11054. (d) Boldrini, B.; Cavalli, E.; Painelli, A.; Terenziani, F. *J. Phys. Chem. A* **2002**, *106*, 6286–6294. (e) Terenziani, F.; Painelli, A.; Girlando, A.; Metzger, R. M. *J. Phys. Chem. B* **2004**, *108*, 10743–10750. (f) Painelli, A.; Terenziani, F.; Angiolini, L.; Benelli, T.; Giorgini, L. *Chem.−Eur. J.* **2005**, *11*, 6053–6063. (g) D'Avino, G.; Grisanti, L.; Guasch, J.; Ratera, I.; Veciana, J.; Painelli, A. *J. Am. Chem. Soc.* **2008**, *130*, 12064–12072. (h) Grisanti, L.; D'Avino, G.; Painelli, A.; Guasch, J.; Ratera, I.; Veciana, J. *J. Phys. Chem. B* **2009**, *113*, 4718–4725.

(47) Terenziani, F.; Painelli, A.; Katan, C.; Charlot, M.; Blanchard-Desce, M. *J. Am. Chem. Soc.* **2006**, *128*, 15742–15755.

(48) (a) Jahn, H.; Teller, E. *Proc. R. Soc. London, A* **1937**, *161*, 220–235. (b) Ham, F. S. In *Electron Spin Resonance*; Geschwind, S., Ed.; Plenum: New York, 1972; pp 1−119.

(49) A Gaussian line shape is used here instead of a Lorentzian, to effectively account for the additional broadening caused by the presence of many coupled vibrational modes with different frequencies rather than the single normal coordinate per molecular arm (a single vibrational frequency) explicitly included in this model.

(50) Liptay, W. *Angew. Chem., Int. Ed.* **1969**, *8*, 177–188.

(51) Painelli, A. *Chem. Phys. Lett.* **1998**, *285*, 352–358.

a slightly different local environment, modeled in terms of a slightly different polar reaction field, resulting in effects that increase with solvent polarity and temperature.

Essential-state models are empirical in nature and all parameters entering the calculation are adjusted for an optimal description of experimental data. The six molecular parameters needed for the calculation of optical spectra are assigned fixed values, independent of the solvent (see Table 1). The solvent polarity is taken into account by tuning a single parameter, the solvent relaxation energy, $\varepsilon_{or}$. The calculated spectra in Figure 1 are obtained with the values listed in Table 1 and setting $\varepsilon_{or} = 0.20$ and 0.27 eV for chloroform and methanol solutions, respectively.

The bottom panel of Figure 1 shows the spectra calculated for CV in chloroform and methanol solutions (red and black, respectively). In both solvents, the linear absorption spectra are in good agreement with the experimental data in the region of the main transition band (I), in terms of position and shape as well as absolute intensity. The intensity of feature II is underestimated in the absorption spectrum, while feature III is clearly beyond the scope of the adopted few-state model. The fluorescence spectrum calculated in methanol compares well with the experimental spectrum. The somewhat underestimated spectral width of the calculated fluorescence spectrum may be related to additional relaxation due to twisting of the phenylene rings or to the presence of several coupled vibrational modes, not included in the present model. The 2PA spectrum calculated in methanol quantitatively reproduces the available experimental data in glycerol,[12] again in terms of position, band shape, and intensity. The maximum TPA cross section is calculated to be about 4000 GM (1 GM = $10^{-50}$ cm$^4$·s·photon$^{-1}$), to be compared with the experimental value of about 2000 GM. A factor of about 2 reduction of the calculated intensity can, however, be easily obtained by accounting for the correction due to the squared refractive index.

The HRS spectra calculated for CV in chloroform and methanol are compared with the experimental data in Figure 1. Apart from a global rescaling of the HRS amplitude (experimental spectra are about 3 times more intense than calculated ones), the calculated spectra are in striking agreement with the experimental ones. As already pointed out for dipolar molecules,[44] the red shift of the HRS main peak with respect to the corresponding 1PA peak is attributed to inhomogeneous broadening in polar solvents. Indeed, the calculated HRS and 1PA spectra peak at the same position when solvation effects are switched off by setting $\varepsilon_{or} = 0$ (see the Supporting Information, Figure S2). However, inhomogeneous broadening has even more intriguing consequences in the present case of octupolar chromophores. In fact, the secondary $\beta$ peak (II) at about 374 nm, clearly related to the activation in the HRS spectrum of the *quasi* one-photon forbidden state, almost disappears in the HRS spectrum calculated for $\varepsilon_{or} = 0$ (see Figure S2 in Supporting Information). This suggests that activation of the forbidden band is mainly due to the lowering of the molecular symmetry, as a result of interaction with the polar surrounding, and is only marginally related to the Herzberg−Teller activation due to the coupling with E-symmetry vibrations. Finally, the $\beta$ peak (III) observed in the calculated HRS spectrum of CV in methanol solution at about 300 nm is a (4 times weaker) replica of the main feature I (see Figure 1). However, the relative intensity of this feature is largely underestimated with respect to the experimental data. The $\beta$ increase in the calculated spectrum can be assigned only to a one-photon resonance with the lowest-energy transition, because the present vibronically coupled essential-state model does not include the 300 nm band observed in the linear absorption spectrum. The intense HRS signal experimentally observed at 300 nm can therefore be assigned to the overlapping one-photon resonance with the lowest-energy absorption band and two-photon resonance with the higher energy excited state at about 300 nm, as was also concluded in the qualitative interpretation above.

Note that, in principle, the same model should also apply to describe vibrational spectra. Indeed, two different frequencies, one related to the two degenerate (E-symmetry) coordinates and one related to the totally symmetric coordinates, are expected to be observed as a result of the different coupling to the electronic system of the two kinds of coordinates. Polar solvation is expected to induce important inhomogeneous broadening effects on bands related to the E-symmetry coordinates (active both in infrared absorption spectra and in Raman spectra), due to the removal of degeneracy in broken-symmetry states. The totally symmetric coordinate, active only in Raman for the symmetric molecule, is expected to be less affected by inhomogeneous broadening effects but can acquire sizable infrared intensity in polar solvents. A detailed analysis of vibrational spectra of CV would, however, require the extension of the model to include multiple coupled modes per arm. As discussed in ref 43 in the context of dipolar dyes, electronic spectra can be accurately described by accounting for just a single effective coupled coordinate that actually accounts for the coupling of several modes to the electronic system. Its frequency corresponds to some average of the frequency of the many coupled modes, and the coupling strength is the sum of the strength of all coupled modes. Indeed, the vibrational frequency adopted here for CV by fitting the linear and nonlinear optical spectra roughly corresponds to an average value of the multiple coupled modes observed in the (hyper-)Raman spectra of CV.[50] Moreover, on the energy scale of the electronic spectra, the precise value of the vibrational frequency is not critical. In contrast, a detailed description of vibrational spectra requires a multimode approach and carefully tuned frequencies. The extension of the model for octupolar chromophores to account for several vibrational modes in each arm, along the lines of ref 43, is possible in principle but leads to a quite cumbersome numerical problem. In fact, the nonadiabatic basis grows as a power of the number of coupled vibrations: accounting for just two modes on each molecular arm would lead to six vibrational coordinates and hence to a very large nonadiabatic basis.

Also the local shape of the two lowest-energy $\beta$ resonances agrees well with the experiment. In particular, the essential-state model calculation confirms the experimental observation that the shoulder in the blue wing of the main $\beta$ resonance (I) is more prominent in methanol than in chloroform. The long-wavelength tail is, however, overestimated by the theoretical model, which may have important consequences for the extrapolated static first hyperpolarizability $\beta_0$. On the basis of our previous study of the $\beta$ dispersion for a dipolar chromophore,[44] this is attributed to the incorporation of too much homogeneous instead of inhomogeneous broadening in the theoretical model. By application of the above-mentioned two-level model of Joffre et al.[8] (eq 4) to the longest-wavelength HRS data point, a static value for $\beta_{HRS}$, $\beta_{0,HRS} = 54 \times 10^{-30}$ esu (corresponding to a $\beta_{0,xxx}$ of $87.5 \times 10^{-30}$ esu) is found for CV in chloroform. The value obtained from the essential-state model for $\beta_{0,HRS}$ is $30 \times 10^{-30}$ esu (almost the same value is obtained in chloroform and in methanol). However, when it is

considered that the theoretical $\beta$ values are systematically lower than the experimental ones, it is most instructive to compare the static values with their respective peak values. For the essential-state model, the static value is 6.3% of the peak value, while the static value estimated by a simple two-level extrapolation (eq 4) from the longest wavelength experimental data point is only 3.35% of the experimental peak value.

**Crystal Violet's Shoulder.** The success of the essential-state model in reproducing a large amount of spectroscopic data in terms of a small set of adjustable parameters demonstrates that the model captures the basic physics of the observed phenomena and can therefore be used to settle a long-standing debate on the origin of the high-energy shoulder in the linear absorption spectrum of CV (at ~550 nm). The shoulder was, for instance, interpreted as a vibronic side band from a single electronic excited state or, alternatively, as due to a second electronic excited state, and it has even been ascribed to the presence of different conformers in solution (for an excellent review see ref 52 and see also the more recent contribution ref 35). Figure S2 in the Supporting Information unambiguously points to a double origin of the side band: the spectrum calculated in the nonpolar solvent (panel a, $\varepsilon_{or} = 0$) in fact shows a small shoulder whose origin is clearly vibronic, as confirmed by the observation of a third vibronic side band. However, the shoulder is much more intense in polar solvents, and in agreement with the experimental data (see Figure 1), it is more resolved in methanol ($\varepsilon_{or} = 0.27$) than in chloroform ($\varepsilon_{or} = 0.20$). Similar effects are observed in HRS spectra, as shown in Figure S2b (Supporting Information). In the same figure (panels c and d), we also report spectra calculated with a truncated nonadiabatic basis ($M = 1$) in such a way that just a single vibronic band can be seen for each electronic transition. In polar solvents, the splitting of the calculated absorption band in two peaks of similar intensity is apparent and can only be ascribed to polar solvation.

While spectra are calculated exploiting vibronic eigenstates obtained via a numerical diagonalization of the nonadiabatic Hamiltonian describing coupled electrons and vibrational degrees of freedom, a more direct understanding of the relevant physics is made possible by the adiabatic solution of the problem. Specifically, in each point of the $F_x$, $F_y$ plane (defined as discussed above by the two components of the solvent reaction field in the molecular plane), we define an adiabatic electronic Hamiltonian fixing the three vibrational coordinates to their local equilibrium position. This is easily done in a self-consistent calculation along the lines briefly described in the Supporting Information. The diagonalization of the adiabatic electronic Hamiltonian in each point of the $F_x$, $F_y$ plane leads to ($F_x$, $F_y$)-dependent energies for the four electronic eigenstates. The resulting energies calculated for CV in methanol are plotted in Figure 4 as a function of $F_x$ and $F_y$ to generate the PES relevant to solvation. The PES corresponding to the ground- and highest-energy states exhibit an almost parabolic behavior: their curvature is related to the elastic restoring force associated with polar solvation. The PESs relevant to the two E-symmetry states are, however, more interesting: the two states are in fact degenerate only at the origin, while the degeneracy is removed for any finite value of the reaction field. One of the E-states undergoes symmetry breaking in polar solvents.

At any temperature, the solution is described as a collection of molecules, each one experiencing a different local field. The

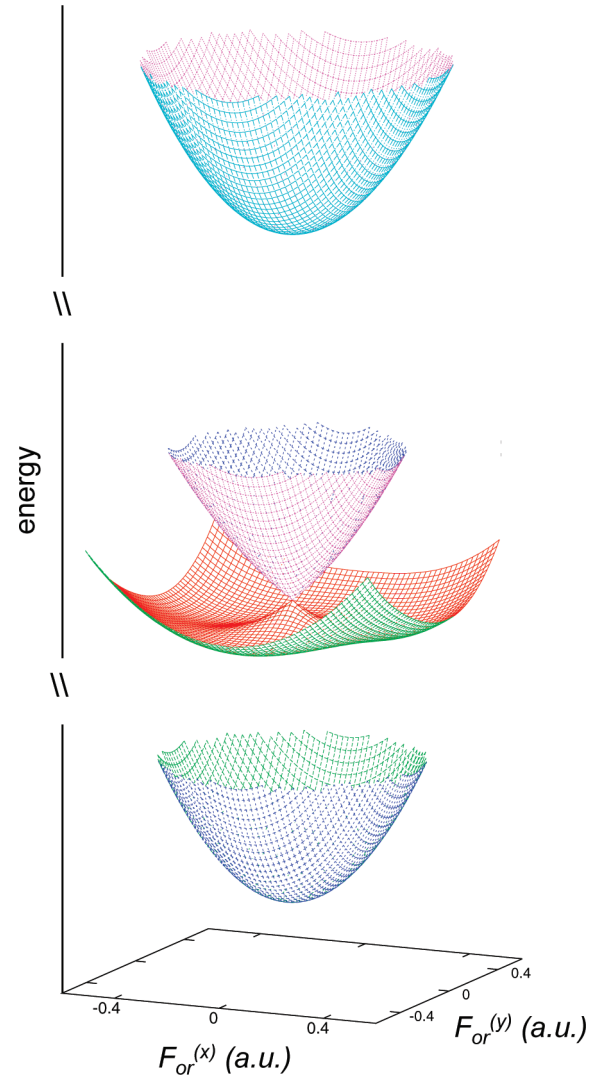


***Figure 4.*** Adiabatic PES for the four essential electronic states, calculated as a function of the two relevant components of the reaction field. Molecular parameters are taken from Table 1 and $\varepsilon_{or}$ is set to 0.27 eV, as relevant for methanol solutions.

probability of the different configurations is governed by the ground-state energy, according to the Boltzmann distribution. The almost harmonic ground-state PES generates a bell-shaped distribution (see Supporting Information, Figure S3), which becomes narrower with decreasing temperature. The distribution peaks at the origin, where the E-symmetry states are degenerate. However, because of the two-dimensional nature of the distribution, areas of larger reaction field get a proportionally larger weight ($\propto|F|$) in the conversion to the corresponding one-dimensional distribution of energies. Therefore, the probability peaks at finite $|F|$, so that the dominant contributions to the absorption and HRS spectra come from molecules experiencing a reaction field of finite magnitude. For these molecules, the degeneracy of the E state is lifted, which explains the observed splitting of the main 1PA and HRS band. This effect is specific to octupolar (two-dimensional) molecules.

To make the discussion more quantitative, the probability distributions for the energies of the excited states calculated for CV in methanol are shown in Figure 5 at room temperature and at 180 K (see Figure S4 in the Supporting Information for the same results in chloroform). Figure 5 shows that indeed, in a polar solvent, the probability of having the two 1E′ states split

(52) Lovell, S.; Marquardt, B. J.; Kahr, B. *J. Chem. Soc., Perkin Trans. 2* **1999**, 2241–2247.

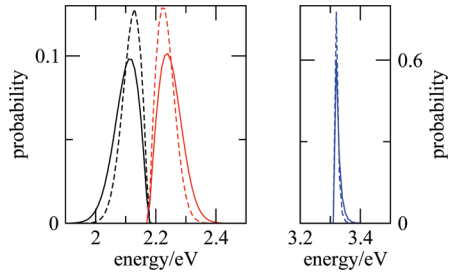


***Figure 5.*** Probability distributions for the essential-state model transition energies to the excited states calculated for CV (molecular parameters in Table 1) with $\varepsilon_{or} = 0.27$ eV (as relevant to methanol) at room temperature (continuous lines) and 180 K (dashed lines). Black and red lines refer to the two E-symmetry states, active in 1PA spectra, and the blue lines refer to the 2PA state.

by about 0.12 eV is much higher than having them degenerate, resulting in a bimodal distribution of the 1E′ energy and thus of the g to 1E′ transition energy. Hence, the two states will mainly absorb at different energies, explaining the main peak and the nearby shoulder observed in the absorption and HRS spectra. This clearly points to the role of disorder introduced by polar solvation as the main origin of the shoulder in the CV spectra. The very narrow distribution of energy calculated for the 2PA state (Figure 5, right panel) is in line with the observation of a very narrow 2PA band,[12] (also confirmed in a very elegant way in ref 22 through the two-photon excitation of the direct emission from that state) and is related to the insensitivity of this symmetrical (nonpolar) and nondegenerate state to the perturbation from polar solvents. We underline that the distributions in Figure 5 are relevant to processes like 1PA, 2PA, and HRS, which involve molecules in their ground state. Fluorescence occurs from the relaxed excited state that, for octupolar chromophores, always corresponds to a broken-symmetry polar state.[28]

Since the $F_x$, $F_y$ solvation fields lower the molecular symmetry (while maintaining the molecular planarity), the $\beta_{HRS}$ reported in Figure 1c has been calculated according to the full SOS expression reported as eq S1 in the Supporting Information. However, similar results are obtained if the truncated $\beta_{HRS}$ expression valid for molecules with $D_{3h}$ symmetry is used (see Figure S1, Supporting Information). This shows that the experimentally accessible quantity $\beta_{HRS}$ offers a reliable estimate of the main component of the molecular hyperpolarizability $|\beta_{xxx}|$.

The energy distributions in Figure 5 are strongly affected by temperature, suggesting nontrivial spectroscopic effects in the absorption band shape. Temperature effects in absorption spectra of CV have been reported previously in other solvents.[53] Figure 6a shows the absorption spectra that we collected for CV in methanol at room temperature and at 180 K (spectra at intermediate temperatures are reported in Figure S5 of the Supporting Information). With decreasing temperature, the band progressively narrows and the shoulder becomes less prominent. Indeed, the spectrum of CV in methanol at 180 K closely resembles the spectrum of CV in chloroform (a less polar solvent than methanol) at room temperature. Figure 6b reports the corresponding calculated spectra. The narrowing and reduction of the shoulder are well reproduced by the essential-state model. Both effects are therefore related to the narrowing of the

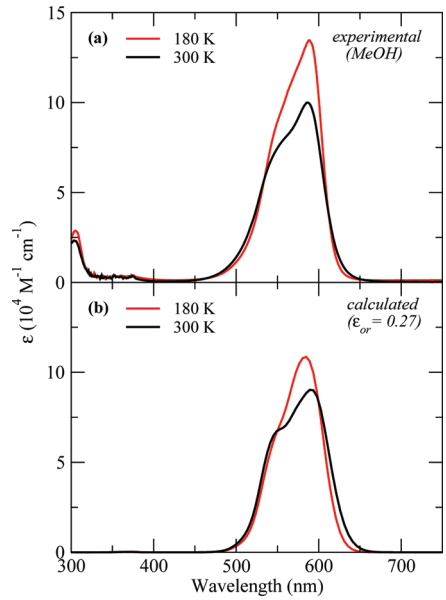


***Figure 6.*** (a) Experimental absorption spectra of CV in methanol at room temperature and at 180 K. (b) Essential-state calculated absorption spectra of CV (molecular parameters in Table 1, $\varepsilon_{or} = 0.27$) at 180 and 300 K. Experimental spectra at intermediate temperatures are reported in the Supporting Information.

probability distribution of the reaction field, with a corresponding decrease of the mean energy splitting between the 1E′ states (see Figure 5). This behavior rules out a purely vibronic origin of the shoulder.

**Quantum-Chemical Calculations.** The vibronic model elaborated above clearly showed that the three excited states included are not sufficient to describe the $\beta$ dispersion for second harmonic wavelengths below 330 nm. However, including more excited states (which would not follow automatically from symmetry) in this model would introduce additional free parameters. Therefore, in order to assess the (purely electronic) resonance contributions from the various excited states quantitatively by means of the SOS expression (eq 3), the transition dipole moments between the various excited states are calculated by means of the coupled-cluster method with single and double excitations (CCSD) implemented in the INDO approach.[54] The homogeneous damping parameters $\gamma$ are set equal for all excited states involved; namely, a value of 0.1 eV has been used as in previous works.[55] These calculations have been performed on the basis of the gas-phase ground-state geometry of CV, as optimized at the density functional theory level (molecular structures were obtained by use of density functional theory with Perdew, Burke, and Ernzerhof (PBE) exchange−correlation functional[56] with a split-valence basis set (SVP);[57] the calculations were performed with the program package Turbomole 6.0[58]). The simulated frequency-dependent $\beta_{HRS}$ is shown in Figure 7. As anticipated, the HRS spectrum of the $D_{3h}$ symmetry

(53) (a) Lewis, G. N.; Magel, T. T.; Lipkin, D. J. *J. Am. Chem. Soc.* **1942**, *64*, 1774–1782. (b) Maruyama, Y.; Ishikawa, M.; Satozono, H. *J. Am. Chem. Soc.* **1996**, *118*, 6257–6263.

(54) Shuai, Z.; Bredas, J. L. *Phys. Rev. B* **2000**, *62*, 15452–15460.

(55) Albota, M.; Beljonne, D.; Bredas, J. L.; Ehrlich, J. E.; Fu, J. Y.; Heikal, A. A.; Hess, S. E.; Kogej, T.; Levin, M. D.; Marder, S. R.; McCord-Maughon, D.; Perry, J. W.; Rockel, H.; Rumi, M.; Subramaniam, C.; Webb, W. W.; Wu, X. L.; Xu, C. *Science* **1998**, *281*, 1653–1656.

(56) Perdew, J. P.; Burke, K.; Ernzerhof, M. *Phys. Rev. Lett.* **1996**, *77*, 3865–3868.

(57) Schafer, A.; Horn, H.; Ahlrichs, R. *J. Chem. Phys.* **1992**, *97*, 2571–2577.

(58) Ahlrichs, R.; Bar, M.; Haser, M.; Horn, H.; Kolmel, C. *Chem. Phys. Lett.* **1989**, *162*, 165–169.

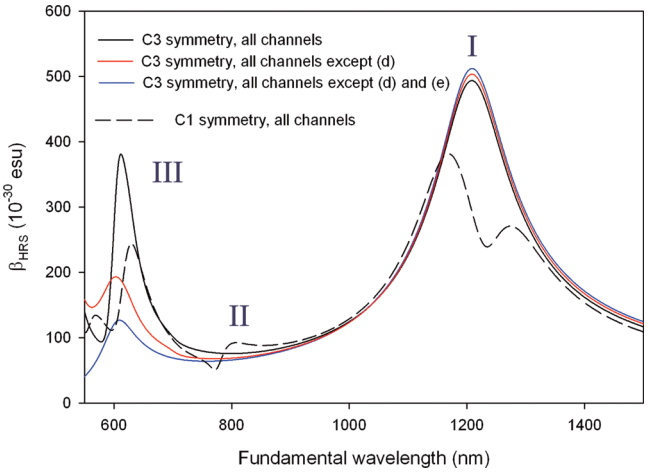


***Figure 7.*** INDO/CCSD/SOS simulated frequency-dependent HRS spectrum for the $D_{3h}$ symmetric CV molecule (solid line) and by artificially breaking the electronic symmetry through the use of a point charge (dashed line). The color lines correspond to the calculated spectrum for the $D_{3h}$ symmetric CV molecule, as obtained by setting to zero contributions from particular channels in Figure 3: d (red line) and d and e (blue line).

compound shows two intense features in the range 0−2.5 eV peaking at fundamental energies (wavelengths) of ∼1 eV (∼1200 nm) and ∼2 eV (∼600 nm). These two bands, assigned as I and III in Figures 1 and 4, are associated with the first and second one-photon optically allowed 1E′ and 2E′ electronic excited states, and their spectral positions and relative intensities are found to be in very good agreement with the HRS measurements (see Figure 1). The main channels contributing to these resonances are illustrated in Figure 3 and qualitatively discussed above. To assess the relative importance of the three channels (c−e in Figure 3), that might, a priori, be expected to give significant contributions to the resonance region III, curves calculated by omitting either one or two of these terms are also presented in Figure 7. This reveals that, in the spectral region of peak III, the almost exactly doubly resonant channel d dominates the HRS response while channels c and e provide smaller and comparable contributions (contribution c amounting to $^1/_4$ the amplitude of resonance I, which originates from the same term, as discussed before). In fact, even though it is expected theoretically, this is, to the best of our knowledge, the first observation of double resonance enhancement through HRS. A previous study, on a dipolar system,[59] failed to observe the expected enhancement of hyper-Rayleigh and hyper-Raman scattering due to double resonance, which was ascribed to a two-level ("dipole") type path dominating in that case, and dephasing of the intermediate state reducing the double resonance contribution. The present calculations also confirm that only in-plane components of the $\beta$ tensor are significant, with all out-of-plane components being at least 2 orders of magnitude weaker than $\beta_{xxx}$. In particular, at the static limit, the calculations yield $\beta_{xxx} = 58 \times 10^{-30}$ esu, while all $\beta_{zij}$ components are below $0.3 \times 10^{-30}$ esu.

As described in the text, the emergence of an intermediate peak in the frequency-dependent HRS signal stems from symmetry breaking effects and can be accounted for quantitatively through the use of the vibronic model developed here. To assess whether these effects are also obtained *qualitatively* from the quantum-chemical calculations, we have performed the same INDO/CCSD calculations while introducing a partial point charge along one of the three arms of the CV molecule (to break the symmetry of the electronic wave functions). More specifically, a point charge of −0.2|e| was placed along the direction of one molecular arm at a distance of 5 Å from the N atom. In line with experiment, the resulting frequency-dependent nonlinear response exhibits a weak intermediate feature at ∼1.5 eV (800 nm) (II in Figures 2 and 7) arising from the partially allowed 2A′ excited state (that dominates the two-photon absorption response of the CV molecule).[12,22] This approach also qualitatively reproduces the splitting of the main resonance (I) upon symmetry breaking.

(59) Leng, W.; Kelley, A. M. *J. Chem. Phys.* **2007**, *127*, 164509.

## Conclusions

In this work, we report the first detailed wavelength-dependent study of the molecular first hyperpolarizability $\beta$ of an octupolar NLO molecule. Making use of two different solvents, highly accurate hyper-Rayleigh scattering (HRS) measurements were successfully performed on the octupolar dye molecule crystal violet (CV) over the broad fundamental wavelength range of 620−1580 nm. Complete correction for broadband multiphoton fluorescence was systematically performed by spectral analysis of the scattered second-harmonic light. The results clearly show that the traditional undamped or homogeneously damped essential-state models are insufficient to describe the NLO response, even for a prototypical and "well-known" octupolar molecule such as CV. Apart from the expected two-photon resonance with the lowest-energy transition, a significant contribution to $\beta$ is observed originating from a nominally one-photon forbidden transition, as well as from an even higher-energy state. The significant contribution from the symmetry-forbidden transition is explained by the fact that although the transition dipole moment between the ground and excited state is small, it is nonzero thanks to the symmetry lowering due to polar solvation, and moreover all the other molecular quantities that determine $\beta$ are very favorable. The experimental results are interpreted in detail by means of the essential-state model for octupolar molecules from ref 28, which takes into account vibronic coupling as well as polar solvation effects. This model yields a correct and consistent description not only of the one- and two-photon absorption spectra and the fluorescence spectra of CV in chloroform and methanol but also of the experimental HRS data. Apart from an overall scaling of the $\beta$ magnitude, the spectral position, shape, and relative amplitude of the two lowest-energy $\beta$ resonances are accurately described with this approach, while the third resonance at ∼300 nm is partially explained.

The essential-state model also naturally explains the shoulder observed in the absorption spectrum (as well as in the HRS spectrum) of CV at ∼550 nm. We demonstrate that this feature, which has been a source of much debate,[35,52] is mainly due to the loss of degeneracy of the 1E′ excited states in polar solvents combined with the two-dimensional nature of the octupolar system. In fact, while the equilibrium reaction field vanishes in view of the nonpolar ground state of the highly symmetric CV structure, thermal fluctuations of the reaction field around the equilibrium lower the molecular symmetry. The consequent splitting of the E-symmetry optically active states shows up with the appearance of a shoulder in both linear absorption and HRS spectra, because the two-dimensional nature of the chromophore effectively gives a larger weight to contributions from finite reaction field magnitudes. These effects are stronger in more

polar solvents and reduce with lowering temperature (i.e., suppressing thermal fluctuations).

Measurements below second-harmonic wavelengths of 330 nm show a sizable contribution beyond the scope of the essential-state model. Quantum chemical calculations by the INDO Hamiltonian and the coupled-cluster method with single and double excitations (CCSD) successfully reproduce the relative intensities of the electronic resonances and indeed identify this third resonance as being dominated by a higher-energy E′ state, which yields a doubly resonant channel via the 1E′ state.

**Acknowledgment.** J.C. is a postdoctoral fellow of the Fund for Scientific Research of Flanders (FWO, Vlaanderen, Belgium). Financial support from the group project G.0129.07 is gratefully acknowledged. The work in Parma is partly supported by the Italian MIUR through PRIN 2006-031511. D.B. is research director of the FNRS.

**Supporting Information Available:** Text and five figures giving details on theoretical calculations, comparison of calculations with/without polar solvation, energy distributions in chloroform, and experimental absorption spectra at other temperatures. This material is available free of charge via the Internet at http://pubs.acs.org.

JA105600T